Imaging Agents

Catching Bubbles: Targeting Ultrasound Microbubbles Using Bioorthogonal Inverse-Electron-Demand Diels–Alder Reactions**

Aimen Zlitni, Nancy Janzen, F. Stuart Foster, and John F. Valliant*

Ultrasound imaging remains one of the most extensively used medical imaging methods because of its high spatial and temporal sensitivity, low cost, and portability and accessibility of equipment. Contrast-enhanced ultrasound using gas-filled microbubbles (MBs) has further enhanced the utility of ultrasound and created the opportunity to employ biomolecule-targeted derivatives for molecular imaging applications.[1] We describe here a new approach to ultrasound molecular imaging that employs the covalent and highly selective capture of functionalized MBs in vitro and in vivo through bioorthogonal inverse-electron-demand Diels–Alder reactions. While pretargeting methods for nanometer-sized materials, such as nanoparticles and liposomes, have been published recently,[2] the work reported herein is, to our knowledge, the first example of the bioorthogonal capture of micron-sized materials and the employment of pretargeting strategies for ultrasound molecular imaging.

Ultrasound contrast agents are generally comprised of an inert gas, such as a perfluorocarbon, surrounded by a lipid, synthetic polymer, or protein shell. The traditional approach to targeting MBs, which are typically 1–8 μm in diameter and therefore restricted to intravascular targets,[3] has been to link biomolecules with a high affinity for a specific protein to the outer shell through covalent bonds (e.g., amide bonds) or strong noncovalent interactions such as biotin–streptavidin binding.[4] These approaches, which have largely exploited antibody and peptide vectors, have demonstrated the ability to selectively localize MBs to sites of angiogenesis, inflammation, and intravascular thrombus formation.[5]

Rather than using targeting vectors to localize conjugated prosthetic groups, new strategies for creating molecular imaging probes are being exploited that employ pretargeting and bioorthogonal coupling chemistry. Here, a targeting vector is administered first, allowing time for localization and

clearance from nontarget organs, followed by a fluorescent or radiolabeled coupling partner that provides a readout for the molecular signal.[6] The inverse-electron-demand Diels–Alder reaction between tetrazines and *trans*-cyclooctene (TCO) is an example of a highly selective and rapid bioorthogonal coupling reaction that has been used successfully to prepare targeted nuclear and optical molecular imaging probes.[7] A comparable strategy for localizing MBs has not been reported. Such a method could offer a way to overcome obstacles to targeting ultrasound contrast agents whose large size and ability to bind only intravascular targets where blood flow rates and shear stress are high, make it particularly challenging to achieve and maintain good contrast in a timeframe that aligns with the limited in vivo stability of MBs.

To test the feasibility of capturing micron-sized bubbles, a novel tetrazine-tagged MB (MB$_{Tz}$) was developed, and its reactivity towards cells treated with a TCO-conjugated anti-vascular endothelial growth factor receptor 2 (VEGFR2) antibody evaluated (Figure 1). VEGFR2 is overexpressed on tumor cells and upon activation triggers multiple signaling pathways that contribute to angiogenesis.[8] The choice of target also allows the use of anti-VEGFR2-tagged MBs (MB$_V$), which were developed by Rychak, Foster, and co-workers for evaluation in preclinical models,[9] to validate the tetrazine–TCO capture methodology.

Tetrazine-functionalized bubbles were prepared using commercially available streptavidin-coated MBs (micro-marker target-ready contrast agents, VisualSonics) and a biotinylated tetrazine. The biotin–tetrazine derivative **5** was synthesized from biotin in four high-yielding steps (Scheme 1). The desired product was ultimately obtained by coupling commercially available 4-(1,2,4,5-tetrazin-3-yl)phenyl)methanamine hydrochloride with 6-biotinamidohexanoic tetrafluorophenyl (TFP) ester (**4**) at room temperature. After semipreparative HPLC, compound **5** was isolated in 75% yield and the product was stable in the freezer for more than six months. The TCO-conjugated antibody (TCO–anti-VEGFR2) was prepared by combining an excess (20 equiv) of commercially available (*E*)-cyclooct-4-enyl-2,5-dioxopyrrolidin-1-yl carbonate (TCO–NHS) with antiVEGFR2 (eBioscience) at 4°C overnight at pH 9.0–9.5. After purification using a 30 kDa centrifugal filter (Amicon Ultra-0.5) MALDI-TOF MS showed an average of 2.8 TCO groups per antibody in the product.

The derivatized bubbles MB$_{Tz}$ and MB$_V$ were prepared by adding **5** or biotinylated antiVEGFR2, respectively, to freshly reconstituted streptavidin-coated MBs. Isolation of the bubbles from the biotin-containing reagents was accomplished by treating the solution with streptavidin-coated magnetic beads (New England Biolabs), which bound residual tetrazine and

[*] A. Zlitni, N. Janzen, Dr. J. F. Valliant
Department of Chemistry and Chemical Biology,
McMaster University
1280 Main St W., Hamilton, Ont., L8S 4M1 (Canada)
E-mail: valliant@mcmaster.ca

Dr. F. S. Foster
Department of Medical Biophysics, University of Toronto,
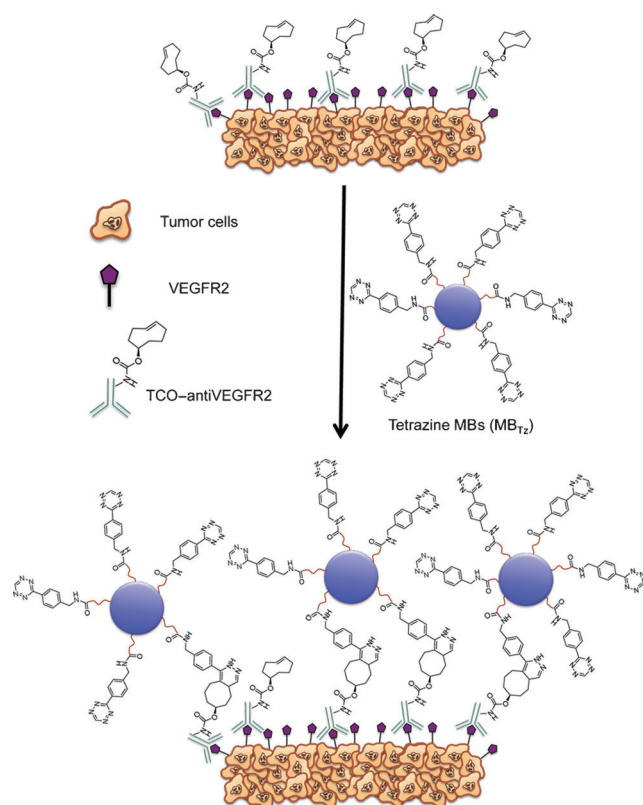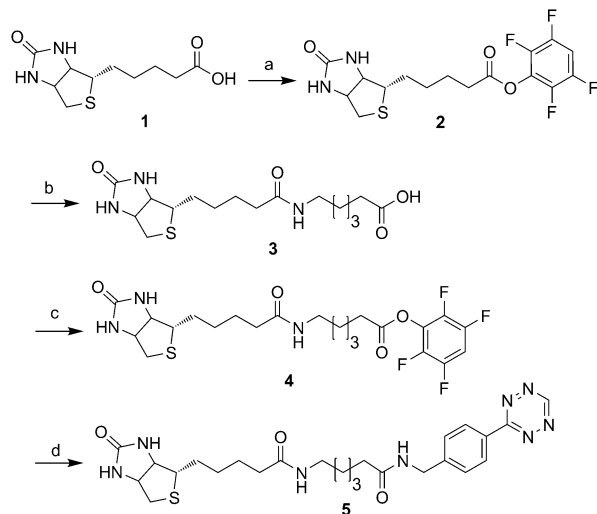Sunnybrook Hospital, Toronto, Ont. M4N S658 (Canada)

Figure 1. Localizing MBs to tumor cells through pretargeting and bioorthogonal chemistry between tetrazine-functionalized microbubbles (MB$_{Tz}$) and an intravascular target (VEGFR2) labeled with a TCO-modified antibody.

Scheme 1. Synthesis of biotin–tetrazine (**5**). Reagents and conditions: a) 2,3,5,6-tetrafluorophenyl trifluoroacetate, DMF, TEA, 30 min, 95%; b) 6-amino-hexanoic acid, DMF, TEA, 75°C, 12 h, 91%; c) 2,3,5,6-tetrafluorophenyl trifluoroacetate, DMF, DMSO, 80°C, 1 h, 96%; d) 4-(1,2,4,5-tetrazin-3-yl)phenyl)methanamine hydrochloride, DMF, TEA, 1 h, 75%. DMF = dimethylformamide, TEA = triethylamine, DMSO = dimethylsulfoxide.

antibody, followed by simple magnetic separation.[10] We found this approach more convenient than centrifugation and washing, as it minimizes the amount of direct handling of the MBs. The bubbles have 7600 molecules of streptavidin µm^{-2}, giving approximately 6000 molecules µm^{-2} of surface area.[9] Prior to working with MB$_{Tz}$, the ability of **5** to bind to VEGFR2-positive H520 cells tagged with TCO–anti-VEGFR2 was evaluated in vitro in direct comparison to a commercially available biotinylated anti-VEGFR2 antibody (biotin–antiVEGFR2). Compound **5** was added to H520 cells that had been incubated with TCO–antiVEGFR2, and the extent of tetrazine–TCO conjugation was determined by adding a FITC-labeled anti-biotin antibody (FITC-antiBiotin) and measuring the arising fluorescence in cell lysates. As a control, FITC–antiBiotin was added to H520 cells that had been incubated with a comparable amount of biotin–anti-VEGFR2. The tetrazine–TCO construct (Figure 2a) showed effectively identical intensity to direct tagging with the biotinylated antibody (Figure 2b). The binding of **5** and FITC–antiBiotin to H520 cells in the absence of any VEGFR2 antibodies was measured and showed significantly lower intensity (Figure 2c), indicating minimal nonspecific binding.
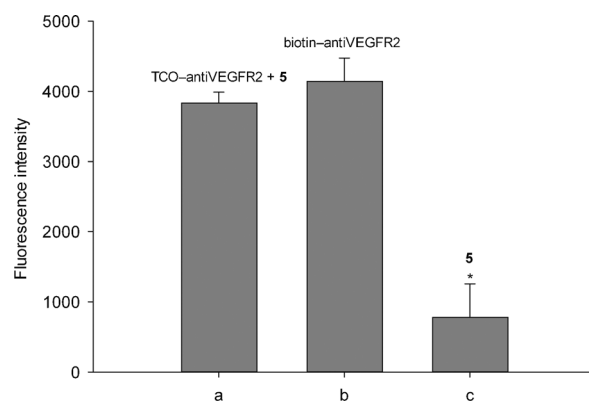

Figure 2. Fluorescence intensity of VEGFR2(+) H520 cell lysates obtained following treatment of cells with a) TCO–antiVEGFR2, **5**, then FITC–antiBiotin; b) commercially available biotin–antiVEGFR2 and FITC–antiBiotin; and c) **5** followed by FITC–antiBiotin. The fluorescence intensity in (a) and (b) were comparable and statistically different (one-way ANOVA) than the control (c). *$p = 0.001$.

To evaluate the effectiveness of the tetrazine–TCO capture strategy, MBs were evaluated initially in vitro under flow conditions (as opposed to simply in culture) similar to those found in tumor capillaries[11] by using a parallel-plate flow chamber system (Glycotech, Rockville, Md.). VEGFR2-expressing cells (H520) and cells lacking VEGFR2 (A431) were incubated with TCO–antiVEGFR2 30 minutes prior to the assay. Using a syringe pump, cells were washed with PBS for 2 minutes to remove any unbound antibody, followed by either functionalized or unmodified MBs for 4 minutes at a 100 s^{-1} shear rate to mimic flow conditions in vivo. To differentiate MBs bound through nonspecific binding interactions from those retained through the TCO–tetrazine

reaction, cells were subsequently washed with PBS for 2 minutes at a 10-fold increased ($1000\,s^{-1}$) shear rate. Optical microscopy was used to visualize the plates and videos were taken during the flow assay and static images for analysis acquired after the final washing step was completed (see the Supporting Information).

Qualitatively, the tetrazine-modified MBs concentrated to a significant extent on H520 cells (VEGFR2(+)) that had been pre-incubated with TCO–antiVEGFR2. The video of the process shows substantially higher retention of MBs over time compared to cells that had not been treated with the antibody (see the Supporting Information). A relatively small amount of MBs bound nonspecifically to the flow chamber during the dynamic component of all assays, which were removed after the final washing step. Images taken subsequently exhibited significant retention of MB_{Tz} (Figure 3a) on
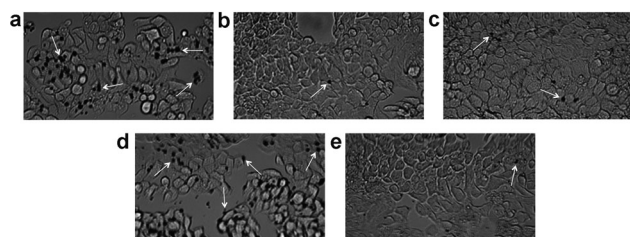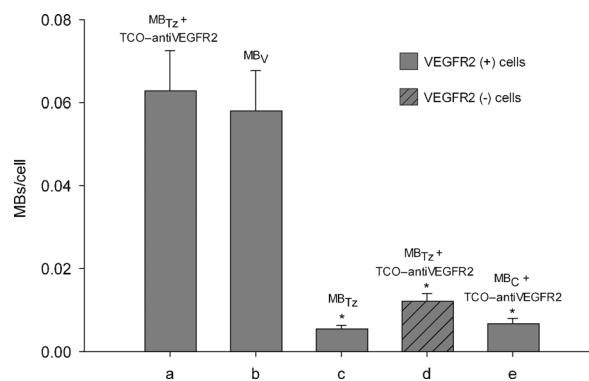

Figure 4. Analysis of the number of MBs bound per cell based on relative area from the flow chamber adhesion assay following washing. For H520 (VEGFR2(+)) cells, near-equivalent binding was seen for a) the MB_{Tz}–TCO–antiVEGFR2 system, and b) anti-VEGFR2-targeted MBs (MB_V). Binding of MB_{Tz} to TCO–antiVEGFR2-tagged H520 cells was significantly higher than with c) unlabeled cells and d) TCO–antiVEGFR2-tagged A431 (VEGFR2(−)) cells ($p = 0.001$). e) Unmodified MBs (MB_C) showed minimal binding to TCO–antiVEGFR2-tagged H520 cells. MB_{Tz} = tetrazine-functionalized MBs; MB_V = MBs functionalized with biotinylated anti-VEGFR2;[9] MB_C = unmodified MBs (micromarker target-ready contrast agents, VisualSonics). Area measurements were determined using FIJI software.[12] * statistically significant difference ($p = 0.001$) relative to (a) (analyzed using one-way ANOVA).

Figure 3. Bright-field microscopy images (20×) showing binding of: a) MB_{Tz} to TCO–antiVEGFR2-tagged H520 cells (VEGFR2(+)); b) MB_{Tz} to H520 cells with no antibody; c) MB_{Tz} to TCO–antiVEGFR2-tagged A431 cells (VEGFR2(−)); d) MB_V to H520 cells; and e) MB_C to TCO–antiVEGFR2-tagged H520 cells. The MBs appear as black spheres with select examples highlighted by the white arrows. MB_{Tz} = tetrazine-functionalized MBs; MB_V = MBs functionalized with biotinylated anti-VEGFR2;[9] MB_C = unmodified MBs (micromarker target-ready contrast agents, VisualSonics).

TCO–antiVEGFR2-tagged H520 cells compared to experiments run with untreated cells (Figure 3b). Repeating the study using VEGFR2-negative A431 cells similarly showed little MB_{Tz} retention (Figure 3c). To compare with more traditional targeting strategies, the VEGFR2-targeted MBs were evaluated under identical conditions and showed comparable binding to the capture strategy (Figure 3d). It was conceivable that TCO–antiVEGFR2 promote nonspecific binding of the MBs to the cells. To test this hypothesis, unmodified MBs as a control (MB_C) were exposed to H520 cells tagged with TCO–antiVEGFR2 and negligible MB retention was observed (Figure 3e).

A semiquantitative analysis was performed by comparing the area covered by the MBs (black spheres) in each image to the area covered by the cells determined using an open-source image processing package.[12] Prior to the analysis, the concentration of the solutions and the sizes of the MBs were determined using a Coulter counter to ensure comparable test conditions. The MB_C, MB_{Tz}, and MB_V concentrations were similar at 5.7×10^6, 6.9×10^6, and 9.4×10^6 $MBs\,mL^{-1}$, respectively, as were the average sizes, at 2.62 ± 0.73, 3.11 ± 0.85, and 2.68 ± 0.73 μm, respectively. MB_{Tz} binding to TCO–antiVEGFR2-tagged H520 cells (Figure 4a) was

more than one order of magnitude higher than its binding to unlabeled cells (Figure 4c). Minimal binding of MB_C to TCO–antiVEGFR2-tagged H520 cells (Figure 4e) and MB_{Tz} to VEGFR2-negative TCO–antiVEGFR2-tagged A431 cells (Figure 4d) was observed, which is consistent with the images shown in Figure 3. The tetrazine system exhibited similar binding to the previously reported antiVEGFR2-targeted MBs (MB_V; Figure 4b), thus indicating that the pretargeting strategy has at least the equivalent ability to localize contrast agent to the VEGFR2 target.

Having demonstrated successful capture on cells under flow conditions similar to those found in tumor capillaries, a preliminary study in animal models was undertaken. Ultrasound imaging was performed using CD1 nu/nu mice bearing SKOV-3 (VEGFR2(+)) human adenocarcinoma tumors. TCO–antiVEGFR2 was administered 24 hours prior to injecting the MBs to allow adequate time for accumulation in the tumor. For consistency with how anti-VEGFR2-targeted MBs (MB_V) were previously assessed, a destruction replenishment sequence[9] was employed four minutes after injection and the differential enhancement of the signal was measured using VevoCQ quantification software (VisualSonics). Regions of interest were based on the vascularity of the tumors determined from the initial distribution of the MBs following injection. All animal experiments were performed following procedures approved by the Animal Research Ethics Board (AREB) at McMaster University.

The images showed high retention of MB_{Tz} in vascularized regions of the SKOV-3 tumors. Even in cases in which the tumors were poorly vascularized (Figure 5a), providing less surface area for capture, contrast enhancement was significant. Contrast was greater than for images obtained in animals that were not administered the antibody (Figure 5b)
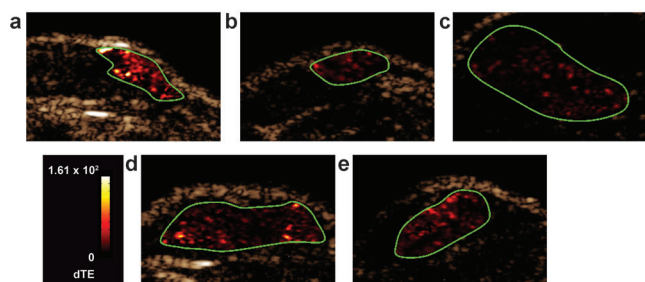
Figure 5. Transverse color-coded parametric nonlinear contrast mode ultrasound images acquired 4 min after intravenous administration of MB$_{Tz}$ to: a) SKOV-3 human adenocarcinoma murine tumor model (VEGFR2(+)) pre-administered with TCO–antiVEGFR2; and b) the same model without antibody; c) A431 human epidermoid carcinoma tumor (VEGFR2(−)) pre-administered with TCO–antiVEGFR2. Images of SKOV-3 murine tumor models following administration of d) MB$_V$; and e) MB$_C$ with pre-administered TCO–antiVEGFR2. Regions of interest were based on the vascularity of the tumors determined from the initial distribution of the MBs following injection. dTE = differential targeted enhancement.

and in A431 (VEGFR2(−)) tumor models despite administration of the antibody (Figure 5c). Localization of the known biotinylated anti-VEGFR2-modified MBs was also apparent (Figure 5d). Interestingly, signals obtained using MB$_C$ on prelabeled SKOV-3 tumors (Figure 5e) was higher than expected but three times lower than with MB$_{Tz}$, suggesting some amount of nonspecific binding.

It is important to note that biotin–streptavidin-based linker systems are not suitable for clinical use because of the immunogenic response caused by multiple injections of streptavidin.[3] However, for clinical applications one can envision preparing a new generation of ultrasound contrast agents that contain tetrazines covalently bound to the shells of MBs in a more biocompatible manner. As ultrasound has emerged as an important preclinical imaging tool, we believe the approach reported here is a general and convenient means of noninvasively evaluating binding of new antibodies to intravascular targets in preclinical models. Bioconjugation of TCO to antibodies or other comparable vectors is simple and reproducible and the associated reagents are commercially available. The corresponding ultrasound images can be obtained using a single type of tetrazine-labeled MB, such as the one reported, eliminating the complexities and variability (i.e., changes in bubble size and extent of functionalization) associated with preparing different antibody–MB derivatives. The approach should therefore expedite the evaluation of different MB-targeting strategies and help accelerate the development of novel ultrasound molecular imaging probes. It also reduces barriers to use ultrasound imaging in order to evaluate new antibody-based therapeutics because targeted MB development and optimization is greatly simplified.

In conclusion, we provided the first evidence that capturing MBs in vitro and in vivo is feasible using bioorthogonal coupling reactions. Taken together, the flow chamber assays and imaging data demonstrate that the localization of MBs is related to the presence of the target (VEGFR2) and the tetrazine–TCO reaction, and not simply the formation of

antibody-labeled bubbles in situ. The comparable binding observed for the bubble-capture strategy and the known VEGFR2-targeted MBs (MB$_v$) further validates that the reported approach can be used to effectively visualize a specific target in both cells under a flow format and animal models. Further use and study of MB-capture strategies appears warranted, with current efforts focusing on evaluating different pretargeting constructs, linker lengths, dosing levels, and timing to further enhance image contrast and create new classes of molecularly targeted ultrasound contrast agents.

[1] O. F. Kaneko, J. K. Willmann, *Quant. Imaging Med. Surg.* **2012**, *2*, 87–97.

[2] a) S. B. Lee, H. L. Kim, H.-J. Jeong, S. T. Lim, M.-H. Sohn, D. W. Kim, *Angew. Chem.* **2013**, *125*, 10743–10746; *Angew. Chem. Int. Ed.* **2013**, *52*, 10549–10552; b) F. Emmetiere, C. Irwin, N. T. Viola-Villegas, V. Longo S. M. Cheal, P. Zanzonico, N. Pillarsetty, W. A. Weber, J. S. Lewis, T. Reiner, *Bioconjugate Chem.* **2013**, *24*, 1784–1789; c) J. Rho, J. Chung, H. Im, M. Liong, H. Shao, C. M. Castro, R. Weissleder, H. Lee, *ACS Nano* **2013**, *7*, 11227–11233; d) S. S. Agasti, R. H. Kohler, M. Liong, V. M. Peterson, H. Lee, R. Weissleder, *Small* **2013**, *9*, 222–227; e) G. Budin, H. J. Chung, H. Lee, R. Weissleder, *Angew. Chem.* **2012**, *124*, 7872–7875; *Angew. Chem. Int. Ed.* **2012**, *51*, 7752–7755; f) C. Tassa, M. Liong, S. Hilderbrand, J. E. Sandler, T. Reiner, E. J. Keliher, R. Weissleder, S. Y. Shaw, *Lab Chip* **2012**, *12*, 3103–3110; g) V. M. Peterson, C. M. Castro, H. Lee, R. Weissleder, *ACS Nano* **2012**, *6*, 3506–3513; h) M. Liong, M. Fernandez-Suarez, D. Issadore, C. Min, C. Tassa, T. Reiner, S. M. Fortune, M. Toner, H. Lee, R. Weissleder, *Bioconjugate Chem.* **2011**, *22*, 2390–2394; i) J. B. Haun, N. K. Devaraj, B. S. Marinelli, H. Lee, R. Weissleder, *ACS Nano* **2011**, *5*, 3204–3213; j) J. B. Haun, N. K. Devaraj, S. A. Hilderbrand, H. Lee, R. Weissleder, *Nat. Nanotechnol.* **2010**, *5*, 660–665.

[3] S. Hernot, A. L. Klibanov, *Adv. Drug Delivery Rev.* **2008**, *60*, 1153–1166.

[4] A. L. Klibanov, *Med. Biol. Eng. Comput.* **2009**, *47*, 875–882.

[5] N. Deshpande, A. Needles, J. K. Willmann, *Clin. Radiol.* **2010**, *65*, 567–581.

[6] a) I. Nikić, T. Plass, O. Schraidt, J. Szymański, J. A. G. Briggs, C. Schultz, E. A. Lemke, *Angew. Chem. Int. Ed.* **2014**, *126*, 2278–2282; *Angew. Chem. Int. Ed.* **2014**, *53*, 2245–2249; b) J. C. T. Carlson, L. G. Meimetis, S. A. Hilderbrand, R. Weissleder, *Angew. Chem.* **2013**, *125*, 7055–7058; *Angew. Chem. Int. Ed.* **2013**, *52*, 6917–6920; c) S. M. van den Bosch, R. Rossin, P. Renart Verkerk, W. ten Hoeve, H. M. Janssen, J. Lub, M. S. Robillard, *Nucl. Med. Biol.* **2013**, *40*, 415–423; d) D. S. Liu, A. Tangpeerachaikul, R. Selvaraj, M. T. Taylor, J. M. Fox, A. Y. Ting, *J. Am. Chem. Soc.* **2012**, *134*, 792–795; e) N. K. Devaraj, R. Weissleder, *Acc. Chem. Res.* **2011**, *44*, 816–827; f) B. M. Zeglis, P. Mohindra, G. I. Weissmann, V. Divilov, S. A. Hilderbrand, R. Weissleder, J. S. Lewis, *Bioconjugate Chem.* **2011**, *22*, 2048–2059; g) N. K. Devaraj, S. S. Hilderbrand, R. R. Upadhyay, R. R. Mazitschek, R. R. Weissleder, *Angew. Chem.* **2010**, *122*, 2931–2934; *Angew. Chem. Int. Ed.* **2010**, *49*, 2869–2872; h) J. C. Jewett, C. R. Bertozzi, *Chem. Soc. Rev.* **2010**, *39*, 1272–1279;

i) N. K. Devaraj, R. Upadhyay, J. B. Haun, S. A. Hilderbrand, R. Weissleder, *Angew. Chem.* **2009**, *121*, 7147 – 7150; *Angew. Chem. Int. Ed.* **2009**, *48*, 7013 – 7016; j) E. M. Sletten, C. R. Bertozzi, *Angew. Chem.* **2009**, *121*, 7108 – 7133; *Angew. Chem. Int. Ed.* **2009**, *48*, 6974 – 6998.

[7] a) R. Rossin, T. Läppchen, S. M. van den Bosch, R. Laforest, M. S. Robillard, *J. Nucl. Med.* **2013**, *54*, 1989 – 1995; b) B. M. Zeglis, K. K. Sevak, T. Reiner, P. Mohindra, S. D. Carlin, P. Zanzonico, R. Weissleder, J. S. Lewis, *J. Nucl. Med.* **2013**, *54*, 1389 – 1396; c) R. Rossin, S. M. van den Bosch, W. Ten Hoeve, M. Carvelli, R. M. Versteegen, J. Lub, M. S. Robillard, *Bioconjugate Chem.* **2013**, *24*, 1210 – 1217; d) Z. Wu, S. Liu, M. Hassink, I. Nair, R. Park, L. Li, I. Todorov, J. M. Fox, Z. Li, J. E. Shively, P. S. Conti, F. Kandeel, *J. Nucl. Med.* **2013**, *54*, 244 – 251; e) E. J. Keliher, T. Reiner, G. M. Thurber, R. Upadhyay, R. Weissleder, *ChemistryOpen* **2012**, *1*, 177 – 183; f) N. K. Devaraj, G. M. Thurber, E. J. Keliher, B. Marinelli, R. Weissleder, *Proc. Natl.*

Acad. Sci. USA **2012**, *109*, 4762 – 4767; g) R. Selvaraj, S. Liu, M. Hassink, C. Huang, L. Yap, R. Park, J. M. Fox, Z. Li, P. S. Conti, *Bioorg. Med. Chem. Lett.* **2011**, *21*, 5011 – 5014; h) R. Rossin, P. R. Verkerk, S. M. van den Bosch, R. C. M. Vulders, I. Verel, J. Lub, M. S. Robillard, *Angew. Chem.* **2010**, *122*, 3447 – 3450; *Angew. Chem. Int. Ed.* **2010**, *49*, 3375 – 3378.

[8] D. J. Hicklin, L. M. Ellis, *J. Clin. Oncol.* **2005**, *23*, 1011 – 1027.

[9] a) J. J. Rychak, J. Graba, C. White, A. M. Y. Cheung, B. Mistry, J. R. Linder, R. S. Kerbel, F. S. Foster, *Mol. Imaging* **2007**, *6*, 289 – 296; b) J. K. Willmann, R. Paulmurugan, K. Chen, O. Gheysens, M. Rodriguez-Pocel, A. M. Lutz, I. Y. Chen, X. Chen, S. S. Gambhir, *Radiology* **2008**, *246*, 508 – 518.

[10] N. Lazarova, P. W. Causey, J. A. Lemon, S. K. Czorny, J. R. Forbes, A. Zlitni, A. Genady, F. S. Foster, J. F. Valliant, *Nucl. Med. Biol.* **2011**, *38*, 1111 – 1118.

[11] R. K. Jain, *Cancer Res.* **1988**, *48*, 2641 – 2658.

[12] J. Schindelin et al., *Nat. Methods* **2012**, *9*, 676 – 682.